A new dynamic inflow model for vertical-axis wind turbines

De Tavernier, Delphine; Ferreira, Carlos S.

DOI
10.1002/we.2480

Publication date
2020

Document Version
Final published version

Published in
Wind Energy

Received: 25 September 2019 | Revised: 23 December 2019 | Accepted: 10 January 2020
DOI: 10.1002/we.2480

WILEY

RESEARCH ARTICLE

A new dynamic inflow model for vertical-axis wind turbines

Delphine De Tavernier | **Carlos S. Ferreira**

Wind Energy Research Institute, Faculty of Aerospace Engineering, Delft University of Technology, Delft, The Netherlands

Correspondence
Delphine De Tavernier, Wind Energy Section, Faculty of Aerospace Engineering, Delft University of Technology, Kluyverweg 1, Delft 2629HS, The Netherlands.
Email: d.a.m.detavernier@tudelft.nl

Abstract

This paper presents a new dynamic inflow model for vertical-axis wind turbines (VAWTs). The model uses the principle of Duhamel's integral. The indicial function of the inflow- and crossflow-induction required to apply Duhamel's integral is represented by an exponential function depending on the thrust coefficient and the azimuthal position. The parameters of this approximation are calibrated using a free wake vortex model. The model is compared with the results of a vortex model and higher fidelity computational fluid dynamic (CFD) simulations for the response of an actuator cylinder to a step input of the thrust and to a cyclic thrust. It is found that the discrepancies of the dynamic inflow model increase with increasing reduced frequency and baseline thrust. However, the deviations remain small. Analysing the application of a finite-bladed floating VAWT with non-uniform loading and validating it against actuator line CFD results that intrinsically include dynamic inflow shows that the new dynamic inflow model significantly outperforms the Larsen and Madsen model (which is the current standard in fully coupled VAWT models) and enhances the modelling of VAWTs.

KEYWORDS

actuator cylinder, CFD, dynamic inflow, floating, VAWT, vortex model

1 | INTRODUCTION

Offshore wind turbine technology has made significant and rapid progress since the first offshore wind farm was installed in 1991.[1] We advanced from fixed platforms to floating structures to be able to overcome deeper water depths. Onshore, horizontal-axis wind turbines (HAWTs) have reached a mature level of technology and dominate the market. Far offshore, the operational conditions are significantly different, raising the question whether other concepts such as vertical-axis wind turbines (VAWTs) could be more suitable and allow a reduction in the cost of energy. The development of floating VAWTs is still at an early stage. A fundamental difference between onshore and offshore turbines is the additional complexity introduced by the motions of the floating platform.[1] Turbines are translating and rotating in three dimensions, as visualised in Figure 1, causing dynamic inflow conditions at the rotor.

1.1 | Background

Dynamic inflow is the phenomena describing the unsteady relation between the induction at the rotor (or any other point of the flow) and the unsteady loading on the rotor and/or unsteady momentum of the flow. As an example, a variation of the loading can be caused by a change in the inflow wind speed and/or a change in for example pitch angle or rotor speed. The change in induction will lag the variation of the loading. The gradual change of the induced velocity from one equilibrium to another is the essential characteristic of the dynamic inflow phenomenon.

In some modelling techniques such as computational fluid dynamics or vortex methods, phenomena like the dynamic inflow effect are represented inherently since the velocity field as a result of a variable force field and/or incoming flow is physically modelled in space and time. However, for fully coupled methods accounting for the aerodynamics, hydrodynamics, structural dynamics, and controller dynamics, these models are too time-consuming making them unsuitable for iterative processes. Simpler momentum-based models are often opted for; however, they need additional correction models to cope with unsteady effects such as dynamic inflow.[2]

Only a few engineering simulation tools are available for the (small but growing) VAWT industry to perform fully coupled unsteady simulations of VAWTs; amongst them are HAWC2,[3] FloVAWT,[4] SIMO-RIFLEX-DMS,[5] and SIMO-RIFLEX-AC.[6] In these fully coupled methods,

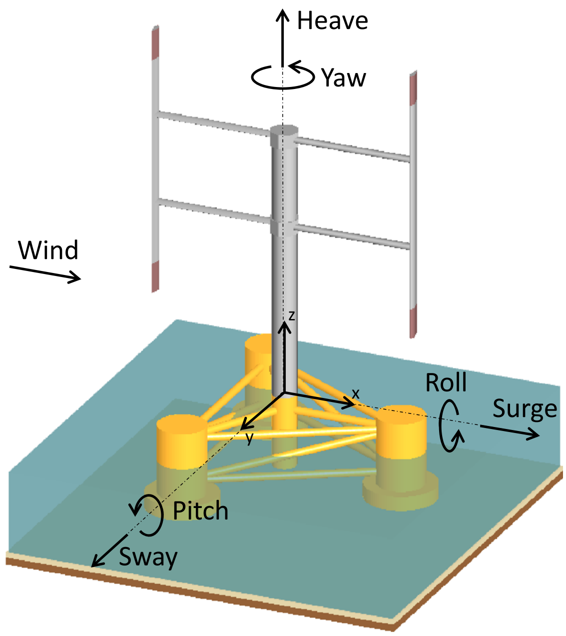

FIGURE 1 Definition of the platform motions [Colour figure can be viewed at wileyonlinelibrary.com]

the aerodynamic modelling is established using the 2D double multiple-streamtube model or the actuator cylinder model. These (quasi-) steady models are augmented with dynamic inflow models. The dynamic inflow models opted for by these researchers are derived for HAWTs. To the knowledge of the authors, there is no dynamic inflow model available particularly derived for VAWTs.

For HAWTs, much effort has already been made in the development of engineering dynamic inflow models. Most models introduce a first-order time derivative ($\tau du/dt$) to the general momentum theory relation between the axial rotor induction and the thrust coefficient.[2] A definition of the time constant τ has been set up by many researchers and is mostly a function of the time and/or radial position. The most common models are the Pitt-Peters model, the Øye model, and the ECN model. The Pitt-Peters model[7] is developed based on the concept of *apparent mass* and uses the analogy of an impermeable disc moving normal to its plane. The Øye model[8] was developed using a vortex ring model, and the ECN model[9] is based on a simplified linear actuator disc model using a prescribed convection velocity. Later, Pirrung and Madsen[10] showed that it is better to use two time constants instead of one. Yu et al[11] recently presented two new dynamic inflow engineering models using two time constants calibrated based on a linear and a non-linear actuator disc vortex model. Van der Deijl[12] showed that there is a difference between dynamic wind and dynamic thrust and proposed an extension of Yu's model.

In previous work,[13] it has been identified that there is a clear difference in the dynamic response of the induction at the different azimuthal positions. This is not considered in dynamic inflow models developed for HAWTs. These models are only calibrated with respect to the rotor disk and thus do not necessarily consider the behaviour upwind and downwind.

1.2 | Research objective

With this motivation, the objective of this paper is as follows:

> "To develop a new engineering dynamic inflow model that enhances the modelling of VAWTs in dynamic inflow conditions."

The paper consists of four parts. First, the main approach is highlighted, and the load cases and modelling techniques used in this work are briefly introduced. Second, a new dynamic inflow model is developed, and the derivation used to set up the model is explained step by step. Third, the results are presented including a comparison of the new dynamic inflow model with respect to higher fidelity models. Fourth, the conclusions are summarised.

2 | METHODOLOGY

2.1 | Approach

VAWTs are often represented by the actuator cylinder concept, in similarity to the actuator disc concept for HAWTs. The actuation surface, coinciding with the swept surface of the rotor, is loaded with the average normal and tangential blade forces occurring during one revolution of the rotor. The development of the new dynamic inflow model builds around this infinite-bladed representation of the VAWT. Because the normal load distribution of a VAWT can basically take any shape depending on variables such as the solidity, tip speed ratio, and blade pitch angle, it is decided to simplify the rotor loading. The average loads on the actuator are prescribed by a simple load distribution mimicking the overall shape of the average loading of a VAWT: a uniform load normal to the actuation surface pointing outwards for the upwind part of the

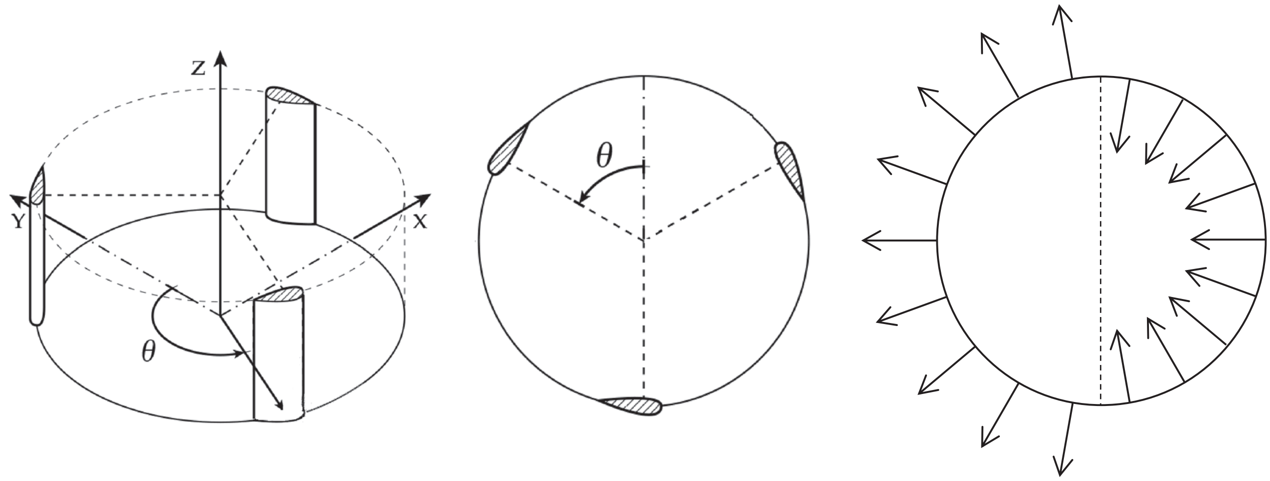

(A) *3D rotor* (B) *2D rotor* (C) *Actuator cylinder*

FIGURE 2 Presentation of the various vertical-axis wind turbine (VAWT) representations and simplifications

rotor and a uniform load normal to the actuation surface pointing inwards for the downwind part of the rotor. No tangential loading is considered since it only marginally affects the induction at the rotor. The new dynamic inflow model, as described in detail in Section 3, is calibrated using a free wake vortex model. The free wake vortex model computes the flow field in space and time over the entire domain and as such simulates dynamic effects intrinsically and with high fidelity.

The derivation and implementation of the new dynamic inflow model is verified by comparing the induction around an actuator cylinder obtained from the dynamic inflow model with the results obtained from the free wake vortex model. Since the results of the free wake vortex model are already used in the calibration, an external CFD model is used as an independent verification method to compute the velocity field around an unsteady actuator cylinder. The unsteady response of a step input in the thrust and a cyclic thrust is studied using the three methods.

Because the new dynamic inflow model is built using a simplified representation of the VAWT with infinite number of blades and a prescribed uniform load distribution, the second validation case study is a finite-bladed VAWT with non-uniform loading in dynamic conditions. The dynamic conditions are realised by introducing a floating motion. For this validation, we compare the results obtained by the Actuator Cylinder model including the new dynamic inflow model and the results obtained from simulations with an actuator line CFD model. The different VAWT representations used in this work are summarised in Figure 2.

2.2 | Study load cases

For the calibration of the new dynamic inflow model as well as the verification and validation of it, different load cases are studied.

- **Load cases for calibration**: For the calibration of the dynamic inflow model, a database of step responses to the thrust of the simplified Actuator cylinder concept is generated using a 2D free wake vortex model. The database is set up for 17 baseline thrust coefficients ranging between 0.1 and 0.9. A step input in C_T of 0.1 is introduced, and the induction response in *x*- and *y*-direction at 60 different azimuthal locations on the actuator is considered. Both a step increase and decrease are analysed. Note that the step input is applied only after a steady solution is found for the baseline thrust coefficient.
- **Load cases for verification and validation**: Besides verifying the dynamic inflow model using the same step inputs to the thrust as used for the calibration of the model (see Section 4.1), the response to a cyclic thrust (see Section 4.2) is studied. Again, the infinite-bladed actuator cylinder with uniform load is considered. The cyclic thrust coefficient is defined by a baseline thrust (C_{T0}), amplitude (ΔC_T), and reduced frequency (k). The cases that are considered in this research have a baseline thrust of 1/9 and 7/9, where the first one presents a low loaded case with a small induction and wake expansion and the second one presents a highly loaded case with a larger induction and considerable wake expansion. The thrust amplitude is fixed to 1/9. The cyclic loading is applied with four different reduced frequencies, ie, 0.05, 0.2, 0.5, and 1. The frequency is non-dimensionalised using $k = \omega R / V_\infty$. The expression of the time-varying thrust coefficient is given by Equation (1). t is the time, R is the radius of the actuator circle, and V_∞ is the incoming wind speed.

$$C_T(t) = C_{T0} + \Delta C_T \cdot \cos\left(\frac{kV_\infty}{R} t\right). \tag{1}$$

The dynamic inflow model is developed for an infinite-bladed uniformly loaded VAWT. To validate that the dynamic inflow model also works in case of a finite-bladed non-uniformly loaded VAWT, simulations are performed for a floating VAWT (see Section 4.3). The analysis of the floating VAWT is adding significant complexity, and this will present the use of the new dynamic inflow model to an application or design case of the VAWT. In this work, only a surging motion (motion in the direction of the wind as shown in Figure 1) is considered. This will cause the velocity perceived by the turbine to be dynamic. The surging motion is prescribed by Equation (2), where s_0 is the baseline surging position, Δs is the surging amplitude, and k is the reduced frequency. The rotor loading is determined using the blade element theory. The baseline surging position is set to 0, and the amplitude to 1 m. The reduced frequencies studied in this work are 0.5, 1, and 2. The surging motions are randomly selected as a way of introducing dynamic inflow and do not necessarily comply with real conditions.

$$s(t) = s_0 + \Delta s \cdot \cos\left(\frac{kV_\infty}{R} t\right). \tag{2}$$

2.3 | Modelling techniques

The approach uses four modelling techniques: a 2D free wake vortex model, an actuator cylinder CFD model, the actuator cylinder model, and the actuator line CFD model. These models are used to analyse the study load cases and are introduced below.

- **2D free wake vortex model (VM)**: Because the 2D actuator cylinder in this paper is uniformly loaded upwind and downwind, vorticity will only be shed at the edges of the actuator or at the transition from upwind to downwind. In fact, the velocity field will be exactly the same as for a 2D uniformly loaded actuator disk, and thus, the surface on which the forces are applied is of non-importance. The time step is set to $0.01R/V_\infty$. This has shown converged solutions. Unsteady variations in C_T are only applied after the steady solution was found for the baseline thrust coefficient. This model will be used to develop and tune the dynamic inflow model.
- **Actuator cylinder CFD model (CFD)**: The computational fluid dynamics (CFD) model of the actuator cylinder concept is built in OpenFOAM.[14] A 2D transient solver for incompressible flows is used, namely, *pisoFOAM*. The predefined thrust coefficient is realised by defining uniformly distributed volume forces over the actuator cylinder region. No turbulence model is applied. The domain has size [−100D, 100D] in width and height. The grid is constructed using blockMesh and is decomposed into a set of one million hexahedral blocks. The grid is dense around the actuator and gradually becomes more course away from the actuator. The time step is set to $0.0025R/V_\infty$. This combination of grid and time step has shown to produce converged results. For the unsteady cases, the initial conditions are defined using the solution of the steady case with a similar baseline thrust. This model will be used as an external validation code of the developed dynamic inflow model for the step in thrust and cyclic thrust load cases for infinite number of blades.
- **Actuator cylinder model (AC)**: The actuator cylinder model, developed by Madsen,[15] is a 2D flow model extending the actuator disk concept. The solution of the velocity field around the actuator cylinder builds on the 2D, steady, incompressible Euler equations and the equation of continuity.[16] It includes a definition for the induced velocities as a function of the volume forces on the actuator surface in the normal and tangential direction. It consists of a linear and non-linear solution. The so-called Mod-Lin solution[3] uses only the linear version of the actuator cylinder model and a correction to account for the non-linear part, instead of solving the computationally expensive non-linear solution. The force field might be determined using an iterative process in which the force field is solved using the blade element theory. The actuator cylinder model is extensively validated and compared against other aerodynamic models by Ferreira et al.[17]

  The actuator cylinder model does not account for unsteady effects and as such should be extended using a dynamic inflow model. So far, the steady actuator cylindermodel has been combined (in, eg, *SIMO-RIFLEX-AC*[6]) with the dynamic inflow model proposed by Larsen and Madsen.[18] In this model, dynamic inflow is modelled using a low pass filtering of the steady state induced velocities. The induced velocity filtered for the near and far wake is presented by Equations (3) to (5) in which a_{n-1} denotes the induced velocity of a previous time step. $a_{s,n}$ refers to the steady induced velocity of the current time step, and Δt is the size of the time step. τ_{nw} and τ_{fw} are the time constants for the near and far wake filter, respectively, and are non-dimensionalised with respect to the rotor radius and average wake velocity ($\tau = \tau^\star R/V_{wake}$). The dimensional constants $\tau^\star_{nw}$ and $\tau^\star_{fw}$ are 0.5 and 2.[19]

$$a_{nw} = a_{n-1}\exp\left(-\frac{\Delta t}{\tau_{nw}}\right) + a_{s,n}\left(1-\exp\left(-\frac{\Delta t}{\tau_{nw}}\right)\right), \tag{3}$$

$$a_{fw} = a_{n-1}\exp\left(-\frac{\Delta t}{\tau_{fw}}\right) + a_{s,n}\left(1-\exp\left(-\frac{\Delta t}{\tau_{fw}}\right)\right), \tag{4}$$

$$a_n = 0.6a_{nw} + 0.4a_{fw}. \tag{5}$$

- **Actuator line CFD model:** The AL model uses the open-source *TurbineFoam* library[20] in OpenFOAM.[14] This model is based on the classical blade element theory and uses a Navier-Stokes description to solve the flow field in space and time. The blades are represented as lines for which the 2D profile lift, drag, and pitching moment are input. The loads are introduced as distributed body forces to the flow field to avoid instability. An extra source term is added to the momentum equation and solved with the pisoFOAM solver. The *TurbineFoam* library includes modules to account for unsteady effects such as dynamic stall, added mass, flow curvature, and end effects[21]; however, they are not considered in this work for simplicity. The model can include struts and a tower, but also these are excluded. For this work, the model is extended to allow turbine motion. The grid is set to $[-8D, 8D]$ in freestream direction, $[-5D, 5D]$ in radial direction, and $[-5D, 5D]$ in spanwise direction and contains 17.5 cells per diameter length. Around the rotor and in the turbulent zone, a first-order refinement of the mesh is applied. The simulations are run for at least 30 revolutions with a time step every 1° azimuthal change. A convergence study on the grid and simulation time step showed that the simulations produced converged results on the power coefficient (variation was below 1E-3). This model will be used to validate that the new dynamic inflow model also works in case of a finite-blade non-uniformly loaded VAWT with the floating motion as extra complexity. The load cases modelled with this code are the cyclic surging VAWT.

When using various models for verification and validation purposes of the dynamic inflow model, it is important to identify and quantify the differences and similarities of the results obtained by the models in absence of dynamic effects. The actuator cylinder model, the actuator cylinder CFD model and the free wake vortex model will be used to calculate the flow field around a simplified actuator cylinder with uniform normal loading upwind and uniform normal loading downwind. In Figure 3, a comparison of the x-induction at the midpoint of the rotor with respect to a steady thrust coefficient is presented. For the vortex model, a maximum difference of 5% is observed up to a C_T of 0.7 compared with the momentum results of the actuator cylinder model. Above a C_T of 0.7, the discrepancies increase. The CFD model agrees well with momentum theory for low thrust. The discrepancy of the induction at the centre of the actuator cylinder is slightly larger for the higher thrust values, with a maximum of 1.5%.

For a three-bladed reference turbine with a solidity of 0.1 and a tip speed ratio of 3, the results are computed using the infinite-bladed actuator cylinder model and the finite-bladed actuator line model. For both models, the blade loading is determined using the blade element theory. The lift and drag are prescribed in both codes by $C_l = 1.11 \cdot 2\pi sin(\alpha)$ and $C_d = 0$. The comparison of the 2D actuator cylinder model is performed with respect to the mid-section of the 3D actuator line OpenFOAM model (with a large aspect ratio of 5) to approach 2D conditions the most. Because both codes are using the same blade element characteristics, all discrepancies can be attributed to the description of the induced velocity. For this reference turbine, the predictions of both codes in steady conditions (excluding dynamic inflow) are very similar. Figure 4 presents a comparison. The azimuthal angle is defined from 0° to 180° in the upwind part of the rotor and from 180° to 360° in the downwind part of the rotor. Q_n is the non-dimensional volume loading normal to the rotor, positive when pointing outwards. Q_t is the tangential volume loading, positive when pointing in the rotational directions. The power and thrust coefficient calculated by the actuator cylinder model are 0.54 and 0.73, respectively. For the actuator line OpenFOAM model, this is 0.52 and 0.72, respectively.

3 | THE DERIVATION OF A NEW DYNAMIC INFLOW MODEL

The development of the new engineering dynamic inflow model for VAWTs is based on the methodology developed in Yu et al.[11] It uses a similar approach as Wagner's model for 2D unsteady airfoil aerodynamics. Duhamel's integral, as given in Equation (6), is used to represent the total induction response of the system to an arbitrary thrust excitation by superimposing the response to step inputs. a_{st} represents the steady induction; Φ is referred to as the indicial response function.

$$a(t,\theta) = a_{st}(0,\theta)\Phi(t,\theta) + \int_0^t \frac{da_{st}(t,\theta)}{d\tau}\Phi(t-\tau,\theta)d\tau. \tag{6}$$

To apply Duhamel's integral, the indicial response needs to be known for all thrust coefficients and azimuthal positions. This process consists of three steps. First, a database is build defining the indicial response of the induction of a 2D actuator cylinder to a step input in the thrust coefficient. The indicial responses are consequently represented by an exponential approximation of which the coefficients are calibrated. Next, a relationship is identified between the coefficients of the exponential approximation on one hand and the thrust coefficient and azimuthal position at the rotor on the other hand. With these relationships known, the indicial response function can be determined for every combination of thrust and azimuthal position, and Duhamel's equation can be employed to solve the unsteady induction at the rotor. Note that in this paper, the presented examples correspond to the *x*-induction, except stated differently.

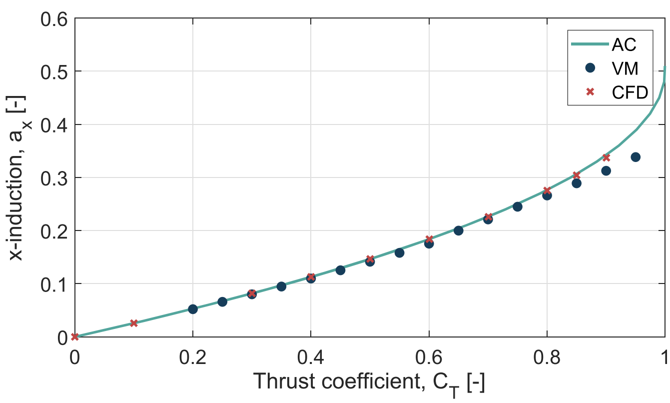

FIGURE 3 The x-induction at the centre of the actuator cylinder with respect to the thrust coefficient from the actuator cylinder model (AC) , free wake vortex model (VM), and the computational fluid dynamic model (CFD) [Colour figure can be viewed at wileyonlinelibrary.com]

3.1 | Database of step responses

The database of step responses is generated using a 2D free wake vortex model. Because vortex models describe the wake in space and time, it captures the unsteady responses intrinsically. The database is set up for various baseline thrust coefficients ranging between 0.1 and 0.9, and the induction response in x- and y-direction at a range of azimuthal locations on the actuator is considered. Both a step increase and decrease in the thrust are analysed on the simplified infinite-bladed actuator cylinder concept. In Figure 5, the (normalised) x- and y-induction responses are provided for three different azimuthal locations. For the x-induction, the most upwind location at $\theta = 90°$, a central location at $\theta = 0°$, and downwind at θ = -90° are considered. Because the y-inductions at the centre line are zero due to symmetry, the response is shown at $\theta = 45°$ and $\theta = -45°$.

3.2 | Indicial function

The indicial step responses of the induction, calculated using the 2D free wake VM, are represented using an exponential approximation using two exponential terms. Similar as found by other researchers such as Pirrung and Madsen[10] and Yu et al[11] two exponential terms seem to be the optimal option since one term is under-fitting and three terms are over-fitting the data. The indicial functions, denoted by Φ, are described by

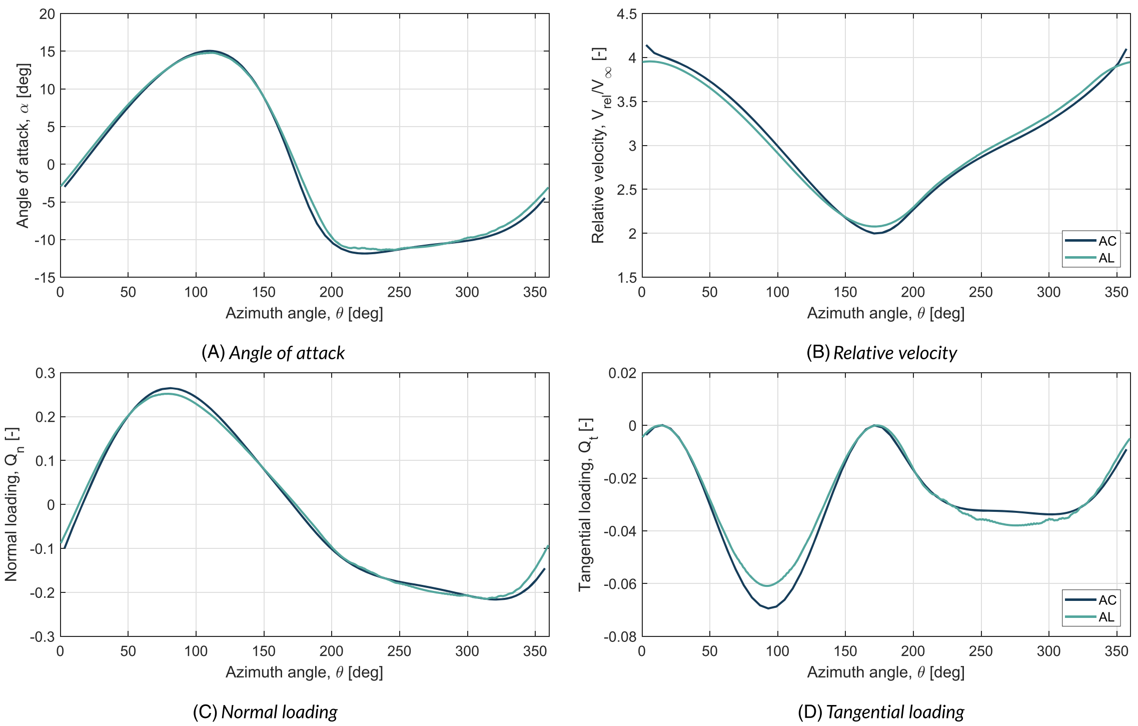

FIGURE 4 Comparison between the actuator cylinder model (AC) and the actuator line OpenFOAM model (AL) for a steady vertical-axis wind turbine (VAWT) with a solidity of 0.1, tip speed ratio of 3.0. $C_l = 1.11 \cdot 2\pi sin(\alpha)$, $C_d = 0$ [Colour figure can be viewed at wileyonlinelibrary.com]

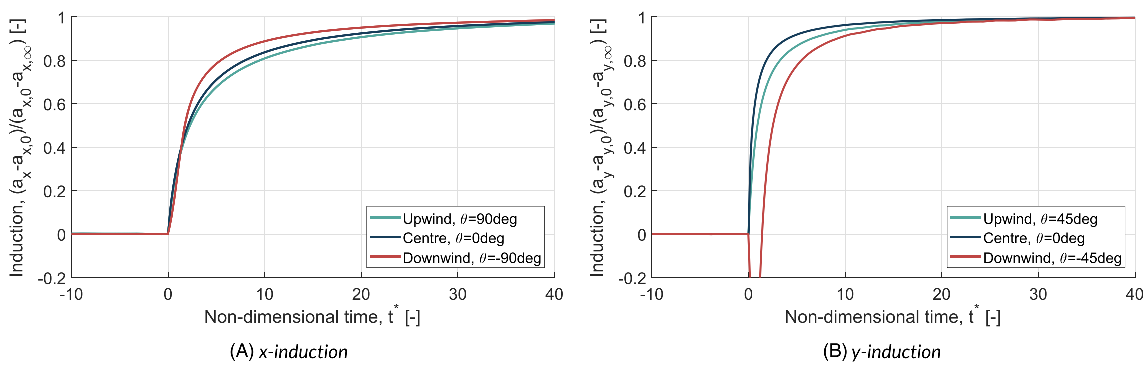

FIGURE 5 Induction response in x and y to a step input in the thrust coefficient from the free wake vortex model (VM). ($C_{T0} = 0.4$, $\delta C_T = 0.1$) [Colour figure can be viewed at wileyonlinelibrary.com]

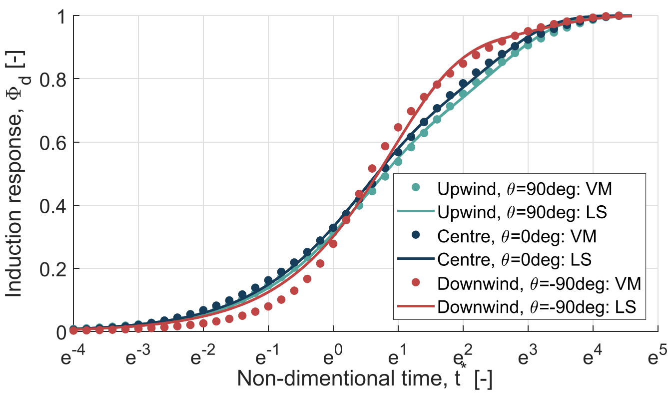

FIGURE 6 Indicial function of x-induction to a step input in the thrust coefficient. *VM* is the result obtained with the Vortex model . *LS* is the least-square exponential approximation ($C_{T0} = 0.4$, $\delta C_T = 0.1$) [Colour figure can be viewed at wileyonlinelibrary.com]

Equation (7). The parameter $t^\star$ is the time non-dimensioned with U_0/R.

$$\Phi(t^\star) = 1 - \beta \cdot e^{\omega_1 t^\star} - (1-\beta) \cdot e^{\omega_2 t^\star}. \tag{7}$$

For every thrust coefficient and azimuthal position with a step increase and decrease in the thrust, the parameters β, ω_1, and ω_2 are determined using a least-square method. The time series is discretised logarithmically to concentrate more time steps right after the thrust coefficient jump. In Figure 6, a representative example is given to show how well the exponential function approximates the indicial responses calculated using the vortex model. Again, three locations are considered: upwind at an azimuthal position of 90°, at the centre at an azimuthal position of 0°, and downwind at an azimuthal position of -90°. As can be understood from the figure, it is difficult to match the response at the downwind location with the exponential function. The reason for this is that for the downwind positions, the new vortices are shed in front of the evaluation point. They effect the evaluation point differently than vortices located behind the evaluation point. It takes time until the first vortices shed after the step input in thrust travel behind the evaluation point. In the x-induction, this behaviour results in a rather steep increase after some time steps. For the y-induction, first a decrease in induction is visible after which it increases to the final value. Although the logarithmic graph might give the impression of large discrepancies, above time step t⋆=0.6, the curves are matching well. For the y-induction, first a decrease in induction is visible after which it increases to the final value. Although the logarithmic graph might give the impression of large discrepancies, above time step $t^\star = 0.6$, t.

3.3 | Coefficients of indicial function

With the coefficients β, ω_1, and ω_2 calibrated for the database, a relation can be identified between the coefficients of the exponential approximation on one hand and the thrust coefficient and azimuthal position on the other hand. Note that the parameters for the step increase and decrease are averaged since they did not show a considerable difference. A polynomial function with the azimuth angle as variable and of order 4 is fit through the upwind data (for $\theta = [10, 170]°$), and a separate polynomial of the sixth order is fit for the downwind part (for $\theta = [190, 350]°$). The upwind and downwind polynomials are connected with a linear fit (for $\theta = [170, 190]°$ and $\theta = [350, 10]°$). The coefficients P_{β_1}, P_{β_2}, $P_{\omega_{11}}$, $P_{\omega_{12}}$, $P_{\omega_{21}}$, and $P_{\omega_{22}}$ are at their turn a function of the baseline thrust coefficient. The equations are provided in Equations (8) and (9). In between the upwind and downwind region, a linear fit is added. The polynomial coefficients are provided in Table 1. In the appendix, Table A1 presents the polynomial coefficients for the y-induction.

$$\text{for} \quad \theta = [10, 170] \cdot \frac{\pi}{180} \tag{8}$$

TABLE 1 The polynomial coefficients of the x-induction as a function of the thrust coefficient to implement in Equations (8) and (9)

	For $\theta = [10,170] \cdot \frac{\pi}{180}$	For $\theta = [190,350] \cdot \frac{\pi}{180}$
$P_\beta(1)$	$-0.0321C_T^2 + 0.0592C_T - 0.0417$	$0.1532C_T^2 - 0.2767C_T + 0.1161$
$P_\beta(3)$	$0.0809C_T^2 - 0.1286C_T + 0.0578$	$-0.1371C_T^2 + 0.3355C_T - 0.1685$
$P_\beta(5)$	$0.1565C_T^2 + 0.1794C_T + 0.3782$	$-0.2825C_T^2 + 0.1670C_T + 0.1132$
$P_\beta(7)$	–	$0.4078C_T^2 + 0.1556C_T + 0.0045$
$P_{\omega_1}(1)$	$0.0153C_T^2 - 0.0240C_T + 0.0091$	$-0.0569C_T^2 + 0.0737C_T - 0.0212$
$P_{\omega_1}(3)$	$-0.0217C_T^2 + 0.0289C_T - 0.0083$	$0.0755C_T^2 - 0.0834C_T + 0.0129$
$P_{\omega_1}(5)$	$-0.0185C_T^2 + 0.0967C_T - 0.1198$	$-0.0176C_T^2 + 0.0594C_T - 0.0429$
$P_{\omega_1}(7)$	–	$0.0925C_T^2 - 0.1159C_T - 0.0151$
$P_{\omega_2}(1)$	$0.0629C_T^2 - 0.1555C_T + 0.0660$	$-0.5942C_T^2 + 0.5817C_T + 0.0124$
$P_{\omega_2}(3)$	$-0.1116C_T^2 + 0.1944C_T + 0.0244$	$1.2446C_T^2 - 1.1680C_T - 0.3157$
$P_{\omega_2}(5)$	$-0.1305C_T^2 + 0.4397C_T - 0.8885$	$-0.4472C_T^2 + 0.4873C_T - 0.1093$
$P_{\omega_2}(7)$	–	$-0.1993C_T^2 + 0.2168C_T - 0.4838$

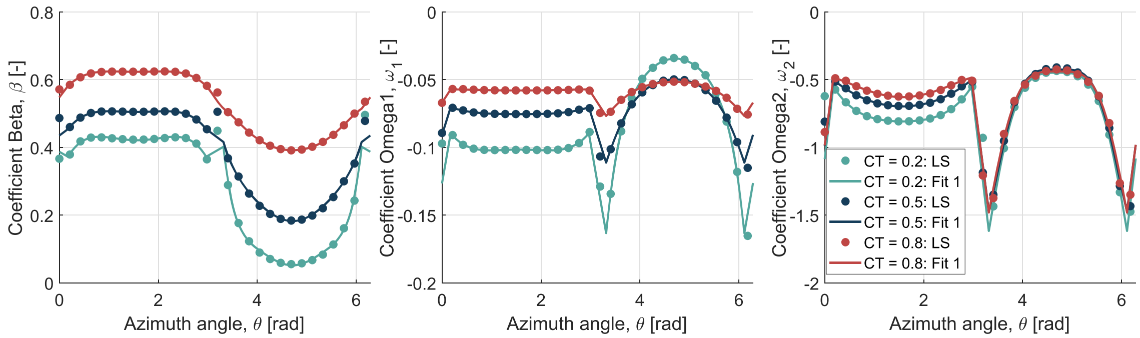

FIGURE 7 Trend between the coefficients β, ω_1, and ω_2 with respect to the azimuth angle for three different thrust coefficients. *LS* are the coefficients obtained from the least-square exponential approximation. *Fit 1* is the polynomial approximation for theta [Colour figure can be viewed at wileyonlinelibrary.com]

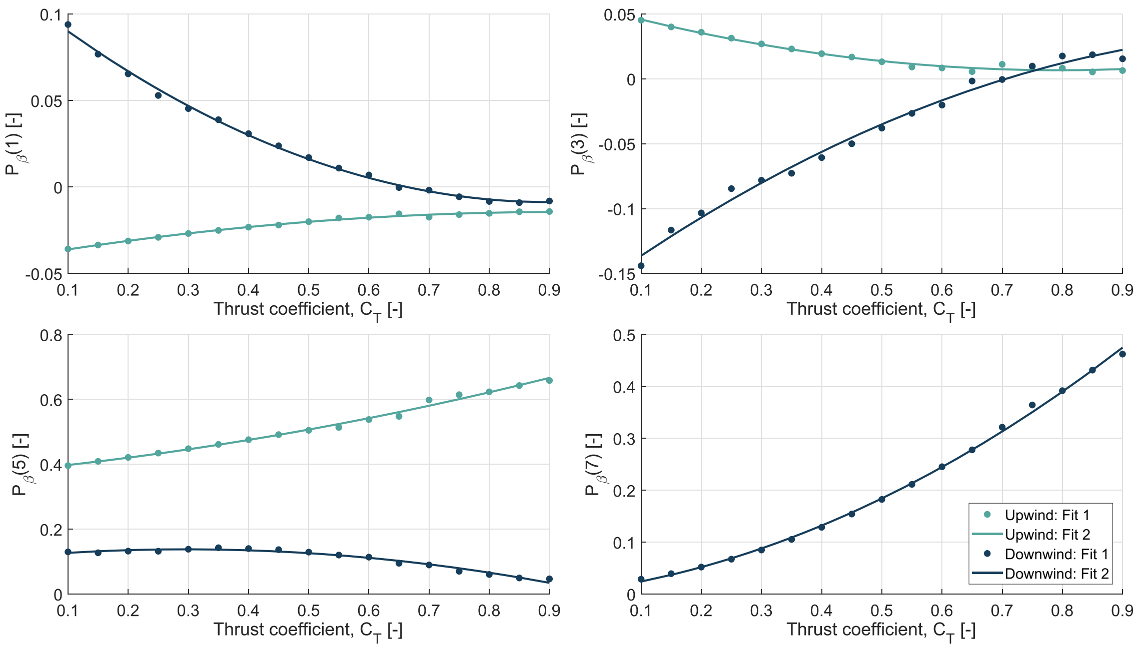

FIGURE 8 Trend between the coefficients P_β and the thrust coefficients. *Fit 1* are the coefficients obtained from the polynomial approximation for theta. *Fit 2* is the polynomial approximation for C_T [Colour figure can be viewed at wileyonlinelibrary.com]

$$\Theta = \theta - \frac{\pi}{2}$$

$$\beta = P_{\beta_1}(5) + P_{\beta_1}(3) \cdot \Theta^2 + P_{\beta_1}(1) \cdot \Theta^4$$

$$\omega_1 = P_{\omega_{1,1}}(5) + P_{\omega_{1,1}}(3) \cdot \Theta^2 + P_{\omega_{1,1}}(1) \cdot \Theta^4$$

$$\omega_2 = P_{\omega_{2,1}}(5) + P_{\omega_{2,1}}(3) \cdot \Theta^2 + P_{\omega_{2,1}}(1) \cdot \Theta^4,$$

$$\text{for} \quad \theta = [190, 350] \cdot \frac{\pi}{180} \tag{9}$$

$$\Theta = \theta - \frac{3\pi}{2}$$

$$\beta = P_{\beta_2}(7) + P_{\beta_2}(5) \cdot \Theta^2 + P_{\beta_2}(3) \cdot \Theta^4 + P_{\beta_2}(1) \cdot \Theta^6$$

$$\omega_1 = P_{\omega_{1,2}}(7) + P_{\omega_{1,2}}(5) \cdot \Theta^2 + P_{\omega_{1,2}}(3) \cdot \Theta^4 + P_{\omega_{1,2}}(1) \cdot \Theta^6$$

$$\omega_2 = P_{\omega_{2,2}}(7) + P_{\omega_{2,2}}(5) \cdot \Theta^2 + P_{\omega_{2,2}}(3) \cdot \Theta^4 + P_{\omega_{2,2}}(1) \cdot \Theta^6.$$

As an example Figures 7 and 8 are provided. In Figure 7, the trend between the exponential coefficients and the azimuthal position is shown for three different thrust coefficients. Also, the polynomial fit is added. The polynomial fit is symmetric explaining why all uneven polynomial terms are cancelled. The fit represents the data well; however, larger deviations are present near the edges of the actuator cylinder. In Figure 8, the relation between the polynomial coefficients and the thrust coefficient is presented for the upwind and downwind region separately. This second fit is only presented for the P_{β_1} and P_{β_2} as a representative example for all parameters.

3.4 | Duhamel's integral

Because now the indicial function is known for every combination of baseline thrust coefficient and azimuthal position, Duhamel's integral can be solved. The application of Duhamel's integral for dynamic inflow assumes that the induction response of an actuator cylinder can be built up as a superposition of responses to a series of step changes. However, because the induction is non-linear with respect to the thrust ($C_T = 4a(1-a)$ according to the momentum theory), this assumption is challenged at high thrust. Duhamel's integral can be solved numerically, as given by Equation (10). At every time step t, a new step change to the thrust is introduced. The response of the induction at time step t is the sum of all responses to the previous step changes introduced at $\tau = [0, t]$ and evaluated at time step t. $d\tau$ is the size from one time step to the other.

$$a(t,\theta) = a_{st}(0,\theta)\Phi(t,\theta) + \sum_{\tau=d\tau}^{t} \frac{a_{st}(\tau,\theta) - a_{st}(\tau - d\tau,\theta)}{d\tau}\Phi(t-\tau,\theta)d\tau. \tag{10}$$

4 | RESULTS AND DISCUSSION

4.1 | Step in thrust

To verify the development and implementation of the new dynamic inflow model, the response of the induction to a step input in the thrust is considered. Because this is the basis of the development of the dynamic inflow model, it is expected that the results match rather well. In Figure 9, a representative example is provided. In this figure, the response of the x-induction in time to a step input of 0.1 is provided for three different locations. The baseline thrust is 0.5 and selected arbitrary. The three locations (upwind at $\theta \approx 45°$, centre at $\theta \approx$ 10° and downwind at $\theta \approx -45°$) show a significantly different indicial function. The results are provided for three codes: (a) the newly developed dynamic inflow model applied to the steady VM results, (b) the free wake VM, and (c) the CFD model. The results of the CFD model serve as external code for further validation. The results show that the step input response is predicted with acceptable accuracy by the dynamic inflow model. The largest deviations are present around a non-dimensional time of $t^* = 5$ for all locations. Similar conclusions can be made for the different baseline thrust cases and the y-induction response as shown in the appendix A1.

4.2 | Cyclic thrust

Because dynamic inflow can be realised by dynamic thrust, a cyclic thrust coefficient is applied on the infinite-bladed AC concept with various baseline thrusts (C_{T0}), amplitudes (ΔC_T), and reduced frequencies (k), as described earlier in the methodology section. In Figure 10, the x-induction is presented at three locations (upwind at $\theta \approx 45°$, centre at $\theta \approx 10°$, and downwind at $\theta \approx -5°$) for a baseline thrust of 1/9, variation of 1/9 and a reduced frequency of 0.5. The results are again presented for the newly developed dynamic inflow model, the VM, and the CFD model as external reference code. The dynamic inflow model is again applied using the results of the VM as steady input values. In general, a good fit can be recognised for all three locations, with a slightly larger deviation at the downwind location. This is true for most cases.

To evaluate this further, other baseline thrust coefficients and reduced frequencies are considered. A range of reduced frequencies is studied going from quasi-steady ($k \leq 0.05$) to moderate unsteady ($0.05 < k \leq 0.2$) and highly unsteady conditions ($k > 0.2$). In order to quantify the hysterical response, the amplitude and phase delay of the induction with respect to the thrust coefficient are calculated using Lissajous' graphical

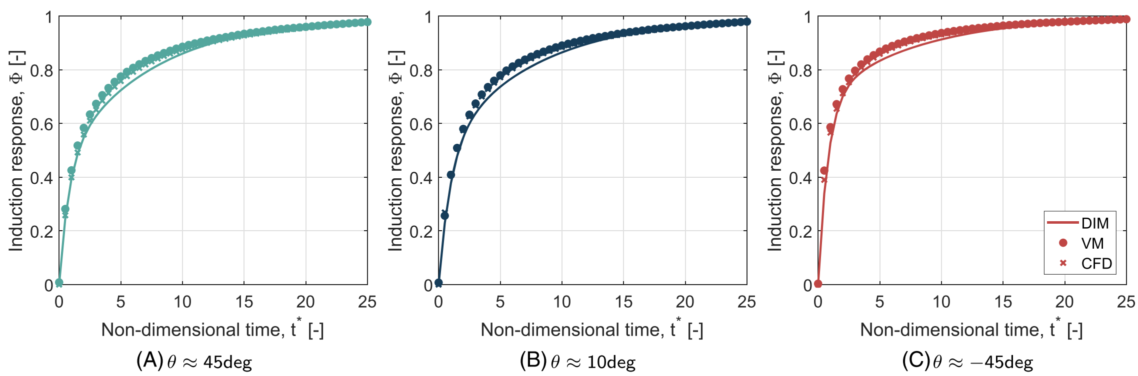

FIGURE 9 Response of x-induction to a step input in the thrust coefficient at three different locations ($C_{T0} = 0.5$, $\delta C_T = 0.1$). *DIM* refers to the results of the dynamic inflow model, *VM* are the vortex model results, and *CFD* are the actuator cylinder CFD results [Colour figure can be viewed at wileyonlinelibrary.com]

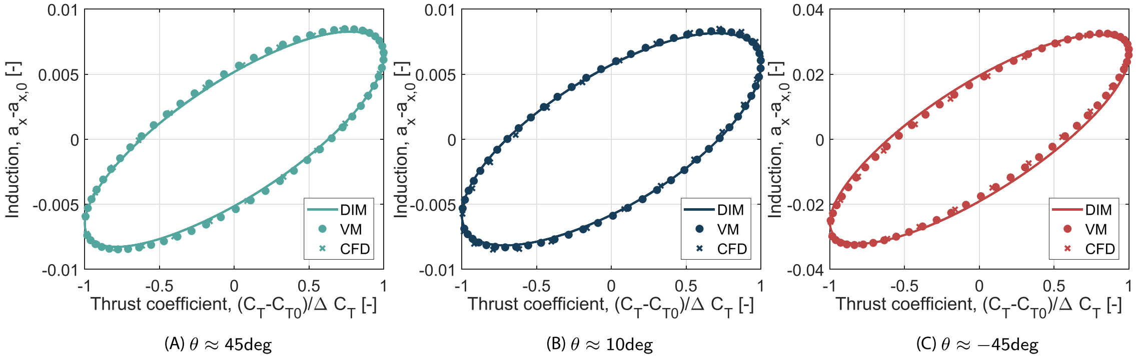

FIGURE 10 Response of x-induction to a cyclic thrust coefficient at three different locations ($C_{T0} = 1/9$, $\delta C_T = 1/9$, $k = 0.5$). *DIM* refers to the results of the dynamic inflow model, *VM* are vortex model results, and *CFD* are the actuator cylinder CFD results [Colour figure can be viewed at wileyonlinelibrary.com]

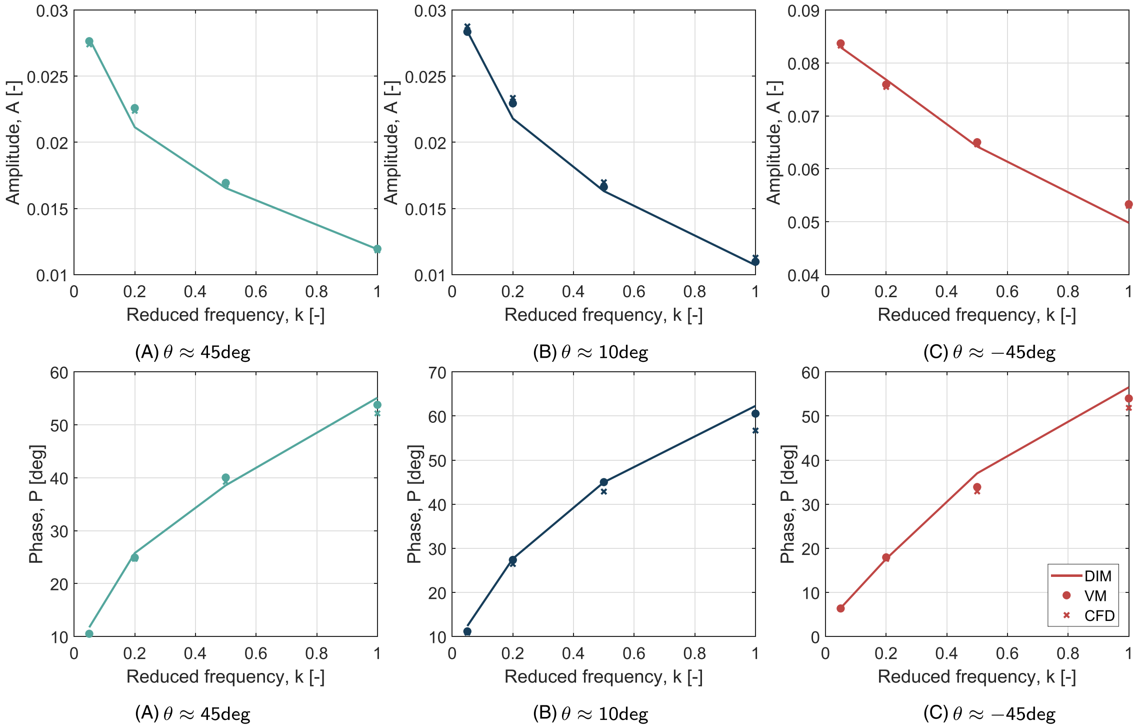

FIGURE 11 Response of x-induction to a step input in the thrust coefficient at three different locations ($C_{T0} = 1/9$, $\delta C_T = 1/9$). *DIM* refers to the results of the dynamic inflow model, *VM*are vortex model results, and *CFD*are the CFD results [Colour figure can be viewed at wileyonlinelibrary.com]

method.[22] Saying that A is the induction amplitude and C is the zero-crossing height, the phase difference Φ between the induction and thrust is given by Equation (11).

$$\Phi = \sin^{-1}\left(\frac{C}{A}\right) \tag{11}$$

The results are presented in Figures 11 and 12 for a baseline thrust of 1/9 and 7/9, respectively. The figures reveal that in general, there is a good match between all three models. For the lowest baseline thrust, the results from the CFD model and vortex model match almost exactly. The error of the newly developed dynamic inflow model with respect to the other models seems to slightly increase with reduced frequency. Also, for the largest baseline thrust, the deviations between the dynamic inflow model and the other models increase with increasing reduced frequency. For the larger baseline thrust, the difference between the vortex model and CFD model is slightly larger. This might be expected since in steady case, it was already observed that the deviations between both models increased for increasing thrust coefficient (see Figure 3). The dynamic inflow model has been calibrated using the results of the vortex model, and therefore, the predictions of the dynamic inflow model are matching slightly better with this model than the CFD model. A slightly lower accuracy is recognised for the downwind location. This could be explained by the fact that the exponential indicial response function for the downwind location was showing larger discrepancies. The fact that the accuracy of the dynamic inflow model decreases with increasing reduced frequency and thrust coefficient could be explained by the fact that the assumptions used in Duhamel's equation are challenged more. For large thrust coefficients, the relationship with the induction is no longer

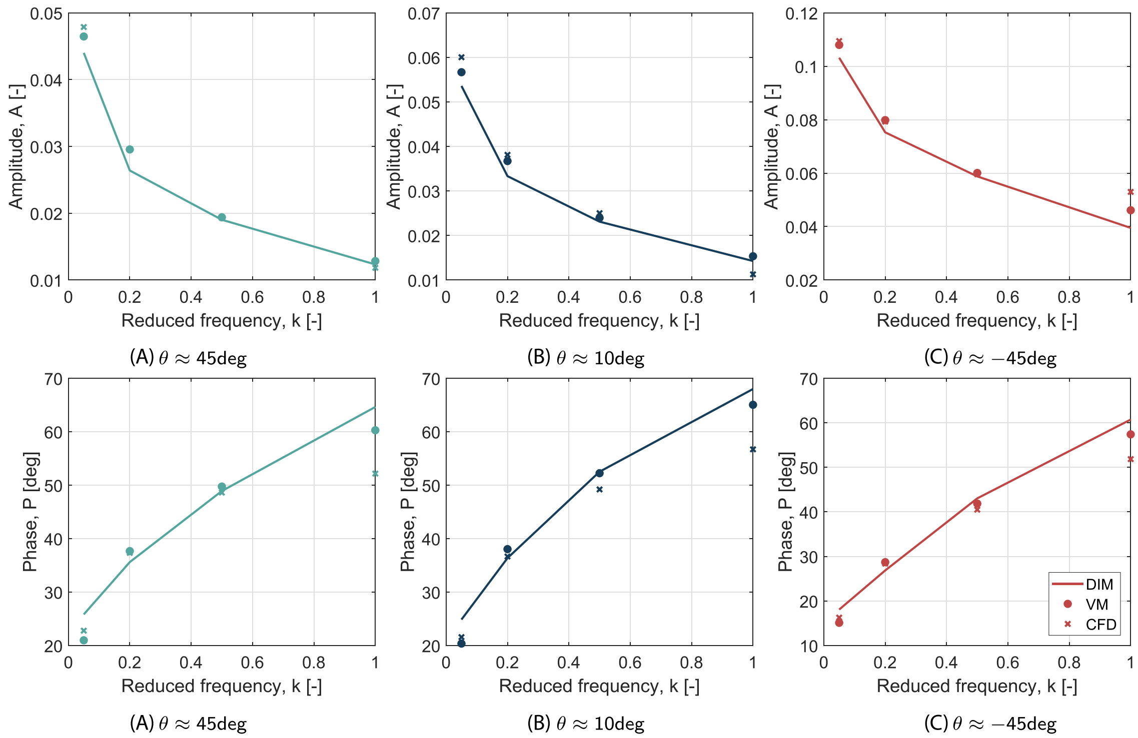

FIGURE 12 Response of x-induction to a step input in the thrust coefficient at three different locations ($C_{T0} = 7/9$, $\delta C_T = 1/9$). *DIM* refers to the results of the dynamic inflow model, *VM*are vortex model results, and *CFD*are the CFD results [Colour figure can be viewed at wileyonlinelibrary.com]

linear. This is one of the assumptions made when applying Duhamel's equation. At large reduced frequencies, the unsteadiness increases, and this is emphasising every error of the model further.

4.3 | Floating VAWT

To validate that the dynamic inflow model, developed for an infinite-bladed VAWT, also works in case of a finite-bladed non-uniformly loaded VAWT, simulations are performed for a cyclic surging VAWT.

The results are computed using four models: (a) the actuator line CFD model, (b) the actuator cylinder model without dynamic inflow model, (c) the actuator cylinder model with the old Larsen and Madsen[18] dynamic inflow model, and (d) the actuator cylinder model with the newly developed dynamic inflow model. The actuator line CFD model serves as reference for this validation since this model intrinsically models dynamic inflow without the use of an extra engineering model. For this validation purpose, it is decided to represent the blades as an actuator line and not geometrically resolve them in the CFD computations. This allows to isolate the discrepancies caused by the modelling of dynamic inflow and as such eliminate errors from other aerodynamic sources such as (amongst others) the errors in the determination of the lift and drag polar or dynamic stall. An actuator line representation allows to use the same blade element properties in all models and to focus the validation only on the dynamic induced velocity. The simulations are performed on a reference turbine with a solidity of 0.1 and a tip speed ratio of 3 in absence of the motion. However, because the surging motion is in fact causing the incoming flow felt by the turbine to vary, a wide range of unsteady tip speed ratios and thus thrust coefficients are tested.

The normal and tangential loadings of all models are presented in Figure 13A and B for a reduced frequency of 1.0. First, it may be argued that the old Larsen and Madsen dynamic inflow model implemented here is capable of capturing the overall trends of the dynamic effects. This model seems to be able to predict the behaviour at the rotor edges well; however, at the most upstream and downstream position, the model still lags accuracy and can be improved further. At some time steps, the AC model without dynamic inflow model outperforms the one including the dynamic inflow model. The new dynamic inflow model, on the other hand, is significantly improved at the time steps that the blade is at the most upwind and downwind position. The overall trend that is shown by the actuator ilne CFD reference model is captured slightly better compared with the old Larsen and Madsen[18] model.

To assess the time response of the actuator cylinder model compared with the actuator line CFD model in a consistent way, the time response assurance criteria (TRAC) is used, as given by Equation (12).[23] This criteria is used for assessing the similarity of two time signals. Values close to 1 indicate high similarity, while values close to 0 indicate low similarity. For the reference turbine without surge motion, the TRAC values of the normal and tangential loading time response are both 0.996, saying that there is a strong similarity between the predictions of the actuator

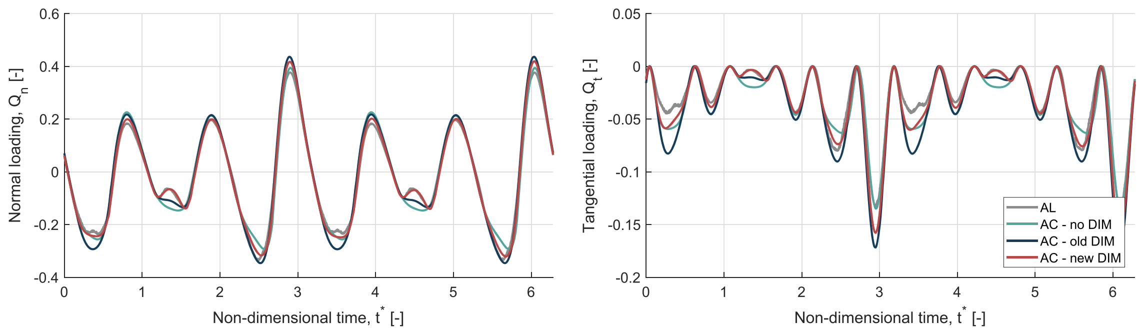

(A) *Normal loading* (B) *Tangential loading*

FIGURE 13 Comparison between actuator cylinder with the new dynamic inflow model (AC - new DIM), with the old dynamic inflow model (AC - old DIM), without dynamic inflow model (AC - no DIM), and actuator line OpenFOAM (AL) model for a vertical-axis wind turbine (VAWT) with a solidity of 0.1 and tip speed ratio of 3.0. Surging motion with $s_0 = 0, \Delta s = 1$. $C_l = 1.11 \cdot 2\pi sin(\alpha), C_d = 0$ at a reduced frequency of $k = 1.0$ [Colour figure can be viewed at wileyonlinelibrary.com]

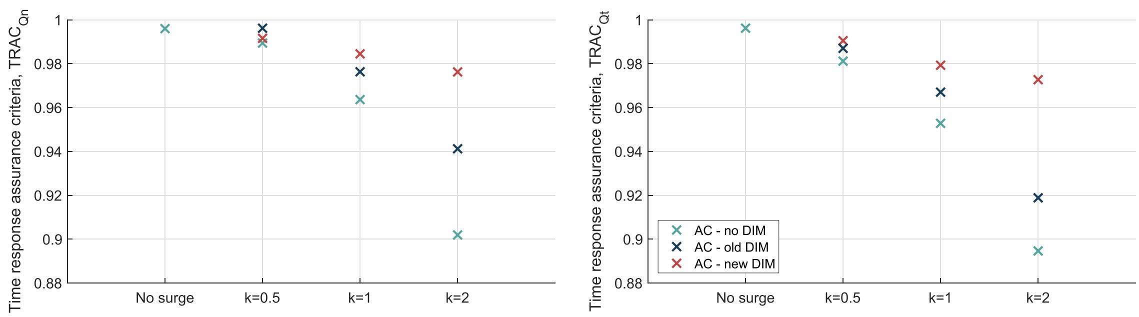

(A) *TRAC normal loading* (B) *TRAC tangential loading*

FIGURE 14 Time response assurance criteria between actuator line OpenFOAM (AL) and actuator cylinder (AC) model with and without dynamic inflow model (DIM) for various reduced frequency on the normal and tangential loading time series [Colour figure can be viewed at wileyonlinelibrary.com]

cylinder model and the actuator line CFD model.

$$TRAC = \frac{\left([t_{AC}]^T[t_{OF}]\right)^2}{\left([t_{AC}]^T[t_{AC}]\right)\left([t_{OF}]^T[t_{OF}]\right)}. \tag{12}$$

The variation of the TRAC value for the actuator cylinder model without dynamic inflow model, with the old Larsen and Madsen[18] dynamic inflow model, and with the new dynamic inflow model for different reduced frequencies is presented in Figure 14. Figure 14A presents the value for the normal loading time series, while Figure 14B considers the tangential loading time series. It is clear that both dynamic inflow models outperform the predictions of the actuator cylinder model without dynamic inflow model. Also, the TRAC value decreases with increasing reduced frequency, confirming that the dynamic inflow effects are larger at larger frequencies.

When comparing the TRAC value of the old and the new dynamic inflow model, one can conclude that the new model outperforms the old one. Only at the reduced frequency of 0.5, the old model is slightly better than the new model if the criteria is applied on the normal loading. However, the values are very close to each other, and the differences in the time series are small. The TRAC value in dynamic conditions is still lower than in steady conditions and decreasing further for more unsteadiness (ie, larger reduced frequency).

It should be remarked that although the dynamic inflow model is also derived for the y-induction, it is of significantly less importance than the x-induction. When not including the dynamic inflow model for the y-induction, there is no visible difference for the normal and tangential loading. The model is mainly derived for completeness.

5 | CONCLUSION

Because wind turbines are often operating in dynamic inflow conditions, it is of great importance to have an accurate engineering dynamic inflow model available. In this paper, a new dynamic inflow model is developed specifically for VAWTs.

The development of the model is based on the methodology presented by Yu et al.[11] and is using the principle of Duhamel's integral. The indicial response functions of the x- and y-induction, required to be able to apply Duhamel's equation, are determined using a three-step process. First, a database is built using a free wake vortex model to define the response to a step input in the thrust coefficient. The indicial responses are consequently approximated by a 2nd order exponential function of which the coefficients are calibrated based on the database. Thirdly, a relationship is identified between the coefficients of the exponential approximation on one hand and the thrust coefficient and azimuthal position at the rotor on the other hand.

The newly developed dynamic inflow model is verified by evaluating the predictions to a step in thrust on the infinite-bladed uniformly loaded actuator cylinder and comparing with the results of the free wake vortex model and a CFD model as independent model. Furthermore, the induction of a 2D actuator cylinder subjected to a cyclic thrust has been compared for various baseline thrust values and reduced frequencies using the same models. It is found that the discrepancies of the dynamic inflow model increase with reduced frequency and baseline thrust; however, the deviations remain small. Also, larger deviations are observed for the downwind location. The deviations can be mainly attributed to the limitations of Duhamel's integral.

Finally, the dynamic inflow model is implemented in the actuator cylinder model and compared against the actuator line CFD model as a way to validate that the model also works in case of a finite-bladed non-uniformly loaded VAWT and enhances the modelling of VAWTs in dynamic inflow conditions. A floating motion is introduced as extra complexity to approach design conditions. Simulations are done for a VAWT in unsteady operation because of a surging motion. The normal and tangential loadings are calculated, and the TRAC values of the loading time series indicate a clear improvement in the predictions in both normal and tangential loadings compared with the predictions performed in absence of a dynamic inflow model and the Larsen and Madsen[18] dynamic inflow model that was originally developed for horizontal-axis wind turbines.

ORCID

Delphine De Tavernier https://orcid.org/0000-0002-8678-8198

REFERENCES

1. Cruz J, Atcheson M. *Floating Offshore Wind Energy: The Next Generation of Wind Energy*. 1st ed. Portugal: Springer; 2016.
2. Schepers JG. Engineering models in wind energy aerodynamics: development, implementation and analysis using dedicated aerodynamic measurements. *PhD thesis*: Delft University of Technology; 2012.
3. Madsen H, Larsen T, Vita L, Paulsen U. Implementation of the actuator cylinder flow model in the HAWC2 code for aeroelastic simulations on vertical axis wind turbines. In: Proceedings of 51st AIAA Aerospace Sciences Meeting including the New Horizons Forum and Aerospace Exposition; Grapevine (Dallas/Ft. Worth Region), Texas; 2013; AIAA2013-0913.
4. Collu M, Borg M, Shires A, Brennan FP. FloVAWT: Progress on the development of a coupled model of dynamics for floating offshore vertical axis wind turbines. In: Proceedings of 32nd International Conference on Ocean, Offshore and Arctic Engineering; 2013; Nantes, France. OMAE2013-10717.
5. Wang K. Modelling and dynamic analysis of a semi-submersible floating vertical axis wind turbine. *PhD thesis*: Norwegian University of Science and Technology; 2015.
6. Cheng Z. Integrated dynamic analysis of floating vertical axis wind turbines. *PhD thesis*; 2016.
7. Pitt DM, Peters DA. Theoreticalprediction of dynamic inflow derivatives. *Vertica*. 1981;5(1):21-34.
8. Øye S. Unsteady wake effects caused by pitch-angle changes, In: Proceedings of the First IEA Symposium on the Aerodynamics of Wind Turbines, London. 1986:58-79.
9. Snel H, Schepers JG. Dynamic inflow: yawed conditions and partial span pitch control. *Report*, Petten: Energy Research Center of the Netherlands; 1995.
10. Pirrung GR, Madsen HA. Dynamic inflow effects in measurements and high fidelity computations. *Wind Energy Science*. 2018;3(2):545-551.
11. Yu W, De Tavernier D, Ferreira C, Kuik GijsAM, Schepers G. New dynamic–inflow engineering models based on linear and nonlinear actuator disc vortex models. *Wind Energy*. 2019;22(11):1433-1450.
12. Van Der Deijl WE. Dynamic wind speed in dynamic inflow models. *Msc thesis*: Delft University of Technology; 2018.
13. De Tavernier D, Ferreira C. The need for dynamic inflow models for vertical axis wind turbines. *J Phys Conf Ser*. 2019;1356:12036.
14. The OpenFOAM Foundation Ltd.. Openfoam v6. https://openfoam.org; 2018.
15. Madsen HA. On the ideal and real energy conversion in a straight bladed vertical axis wind turbine. *PhD thesis*: Aalborg University; 1983.
16. Katz J, Plotkin A. *Low-Speed Aerodynamics*. 2nd ed. United States of America: Cambridge University Press; 2001.
17. Ferreira CS, Madsen HA, Barone M, Roscher B, Deglaire P, Arduin I. Comparison of aerodynamic models for vertical axis wind turbines. *J Phys Conf Ser*. 2014;524:12125.
18. Larsen TJ, Madsen HA. On the way to reliable aeroelastic load simulation on VAWT's. *Proc EWEA*. 2013.
19. Cheng Z, Madsen HA, Gao Z, Moan T. A fully coupled method for numerical modeling and dynamic analysis of floating vertical axis wind turbines. *Renew Energy*. 2017;107:604-619.
20. Bachant P, Goude A, Wosnik M. Turbinesfoam/turbinesfoam: v0.0.8, zenodo. http://doi.org/10.5281/zenodo.1210366; 2018.
21. Bachant P, Goude A, Wosnik M. Actuator line modeling of vertical-axis turbines. arXiv 1605.01449v4; 2018.
22. Al-Khazali HAH., Askari MR. Geometrical and graphical representations analysis of Lissajous figures in rotor dynamic system. *IOSR J Eng*. 2012;2(5):971-978.
23. Chipman C, Avitabile P. Expansion of transient operating data, In *proceedings of the twenty-seventh international modal analysis conference, Orlando, February 2009*.

How to cite this article: De Tavernier D, Ferreira CS. A new dynamic inflow model for vertical-axis wind turbines. *Wind Energy*. 2020;23:1196-1209. https://doi.org/10.1002/we.2480

APPENDIX A

TABLE A1 The polynomial coefficients of the y-induction as a function of the thrust coefficient to implement in Equations (8) and (9)

	For $\theta = [10, 170] \cdot \frac{\pi}{180}$	For $\theta = [190, 350] \cdot \frac{\pi}{180}$
$P_\beta(1)$	$0.0678C_T^2 - 0.1152C_T + 0.0365$	$3.3005C_T^2 - 3.7066C_T + 0.4682$
$P_\beta(3)$	$-0.0258C_T^2 + 0.0590C_T - 0.0280$	$-6.3708C_T^2 + 6.9982C_T - 0.9000$
$P_\beta(5)$	$0.2523C_T^2 - 0.0187C_T + 0.2187$	$-4.7252C_T^2 + 6.3569C_T - 2.5408$
$P_\beta(7)$	–	$9.6071C_T^2 - 13.7709C_T + 6.5173$
$P_{\omega_1}(1)$	$-0.0583C_T^2 + 0.0620C_T - 0.0195$	$-0.5123C_T^2 + 0.4278C_T - 0.1372$
$P_{\omega_1}(3)$	$-0.0205C_T^2 + 0.0917C_T - 0.0455$	$1.2303C_T^2 - 1.0721C_T - 0.2882$
$P_{\omega_1}(5)$	$-0.1476C_T^2 + 0.2974C_T - 0.2124$	$-0.5851C_T^2 + 0.8549C_T - 0.0818$
$P_{\omega_1}(7)$	–	$-0.4953C_T^2 + 1.1874C_T - 0.8920$
$P_{\omega_2}(1)$	$-0.4837C_T^2 + 0.6033C_T - 0.2818$	$-20.2490C_T^2 + 13.6816C_T + 2.2303$
$P_{\omega_2}(3)$	$-0.7813C_T^2 - 0.7053C_T + 0.1054$	$60.2296C_T^2 - 34.0941C_T - 6.3615$
$P_{\omega_2}(5)$	$-0.4974C_T^2 + 0.9831C_T - 1.2059$	$-39.9289C_T^2 + 18.1683C_T - 6.2243$
$P_{\omega_2}(7)$	–	$4.0569C_T^2 - 6.2243C_T - 0.9466$

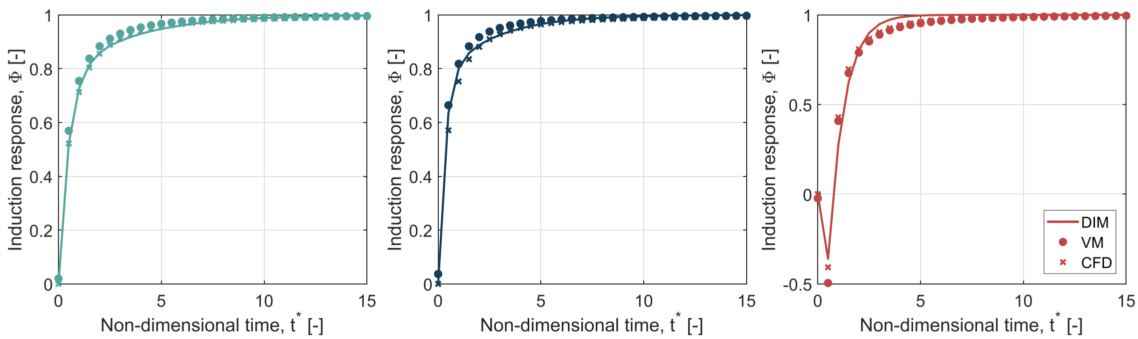

(A) $\theta \approx 45$deg (B) $\theta \approx 10$deg (C) $\theta \approx -45$deg

FIGURE A1 Response of y-induction to a step input in the thrust coefficient at three different locations ($C_{T0} = 0.5$, $\delta C_T = 0.1$). *DIM* refers to the results of the dynamic inflow model, *VM* are vortex model results, and *CFD* are the actuator cylinder CFD results [Colour figure can be viewed at wileyonlinelibrary.com]